AGU PUBLICATIONS

Geophysical Research Letters

RESEARCH LETTER
10.1002/2017GL073079

**Key Point:**
- Wind-driven pond expansion on Mississippi River Delta Plain is leading to land loss

**Supporting Information:**
- Supporting Information S1
- Table S1

**Correspondence to:**
A. C. Ortiz,
aortiz4@ncsu.edu

**Citation:**
Ortiz, A. C., S. Roy, and D. A. Edmonds (2017), Land loss by pond expansion on the Mississippi River Delta Plain, *Geophys. Res. Lett.*, *44*, 3635–3642, doi:10.1002/2017GL073079.

Received 17 DEC 2016
Accepted 30 MAR 2017
Accepted article online 3 APR 2017
Published online 24 APR 2017



# Land loss by pond expansion on the Mississippi River Delta Plain

**Alejandra C. Ortiz[1,2], Samapriya Roy[3], and Douglas A. Edmonds[1]**

[1]Department of Earth and Atmospheric Sciences, Indiana University Bloomington, Indiana, USA, [2]Department of Civil, Construction, and Environmental Engineering, North Carolina State University, Raleigh, North Carolina, USA, [3]Department of Geography, Indiana University Bloomington, Indiana, USA

**Abstract** The world's river deltas may collapse under the combined effects of rising sea levels, subsidence, and reduced sediment supply. Saving these deltaic environments requires quantifying processes driving collapse. In the Mississippi River Delta, rapid land loss offers an important opportunity to test existing theories for marsh collapse. We use Landsat images to examine how pond expansion by edge retreat contributes to land loss over 34 years in the Atchafalaya-Vermillion, Terrebonne, and Barataria basins of the Mississippi Delta. Tracking the area changes in ponds on the marsh surface, we find a striking consistency between pond expansion direction and the dominant wind direction and show that wind-generated waves are capable of causing edge erosion. Expansion rate increases rapidly for ponds wider than 300 m in Terrebonne and Barataria basins. From this, we suggest that ponds in Atchafalaya-Vermillion basin are stable, whereas ponds in Terrebonne and Barataria are unstable.

## 1. Introduction

The Mississippi River Delta is one of the most threatened deltas on Earth and, on average, a football field's worth of land disappears every hour. Given the importance of the Mississippi Delta, it is vital to understand the processes driving marsh collapse of the delta plain. The Mississippi River Delta Plain (MRDP) is experiencing land loss because dam and levee construction on rivers have stopped marshes from receiving the sediment that offsets relative sea level rise [*Blum and Roberts*, 2012; *Edmonds*, 2012; *Twilley et al.*, 2016]. Saving this landscape requires restoration strategies, but success depends on defining and reversing the processes leading to land loss.

Natural land loss on the MRDP mostly occurs from marsh drowning by rising relative sea level or from marsh edge erosion by waves impacting bays, lagoons, or ponds on the marsh surface [*DeLaune et al.*, 1994; *Nyman and DeLaune*, 1999; *Penland et al.*, 2000; *Morton et al.*, 2003; *Craft et al.*, 2009; *Blum and Roberts*, 2012; *Couvillion and Beck*, 2013; *Mariotti and Fagherazzi*, 2013; *Allison et al.*, 2017]. While marsh drowning has occurred locally in the MRDP [*DeLaune et al.*, 1994; *Morton et al.*, 2003], total marsh collapse from drowning is relatively uncommon because positive feedbacks between marsh vegetation and sedimentation minimize marsh vulnerability to drowning [*Morris et al.*, 2002; *Kirwan and Megonigal*, 2013; *Kirwan et al.*, 2016]. Recent work has focused on how increasing connectivity of waterways between ponds increases marsh land loss [*Schepers et al.*, 2017]. Similarly, marsh collapse can occur if water bodies (ponds) on the marsh surface enter a runaway expansion phase [*Nyman et al.*, 1994; *Nyman and DeLaune*, 1999; *Reed*, 2002; *Fagherazzi et al.*, 2013]. Runaway expansion occurs when ponds are greater than some critical width, because edge erosion by waves increases the fetch (or pond width), which increases the wave size, and further increases edge erosion [*Mariotti and Fagherazzi*, 2013; *Mariotti*, 2016]. Ponds smaller than some critical width can maintain their size or disappear [*Wilson et al.*, 2014; *Mariotti*, 2016].

Our goal is to understand pond behavior on the MRDP—that is, whether they are expanding, contracting, or unchanging—and to determine if the MRDP is susceptible to runaway pond expansion. We conducted a remote sensing study of pond behavior from 1982 to 2016 on three basins in the MRDP, Atchafalaya-Vermillion, Terrebonne, and Barataria, because they have varying degrees of land loss and human manipulation [*Blum and Roberts*, 2012; *Twilley et al.*, 2016] (Figure 1a). The Atchafalaya Basin has received continuous sediment delivery through time [*Blum and Roberts*, 2012], whereas Terrebonne and Barataria basins had water and sediment cutoff in 1903 [*Twilley et al.*, 2016].

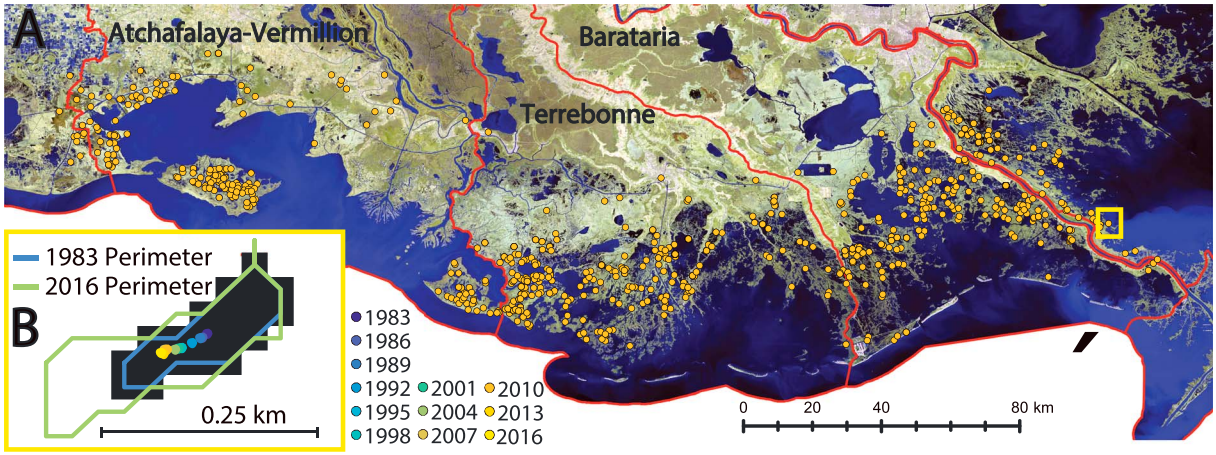


**Figure 1.** Locations of the 730 ponds tracked in this study. (a) The three study basins are outlined in red and labeled [*Twilley et al.*, 2016] with centroids of tracked ponds in orange. The basemap is 2014 composite map of the MRDP from Landsat 8. The image is in false color (bands 7, 6, and 4). (b) Example of pond behavior from the eastern edge of Barataria (yellow box). Centroid position of the pond is plotted from 1983 (dark blue) to 2016 (yellow) along with the change in perimeter.

## 2. Methods

### 2.1. Creation of Composite Images

To identify and track ponds from 1982 to 2016, we create 3 year median Landsat composites for each MRDP basin. The Landsat composites are the per band, per pixel median of all noncloudy pixels for every Landsat 4, 5, 7, and 8 scene over a 3 year period [*Flood*, 2013], computed within Google Earth Engine [*Moore and Hansen*, 2011; *Team*, 2015; *Dong et al.*, 2016]. We use the per pixel median value because it is insensitive to outliers [*Roy et al.*, 2010; *Moore and Hansen*, 2011; *Griffiths et al.*, 2014; *Donchyts et al.*, 2016a, 2016b]. We create composite images over 3 year spans to avoid variable water level and vegetation conditions associated with single scenes at different times. Each composite is transformed into the modified normalized difference water index [*McFeeters*, 1996; *Xu*, 2006; *Rokni et al.*, 2014; *Gautam et al.*, 2015] and is corrected for illumination and contrast differences before final binarization into land-water maps via *Otsu* [1975]. A more detailed discussion of composite image methodology can be found in the supporting information [*Chander et al.*, 2009; *Kuleli et al.*, 2011; *Steyer et al.*, 2013; *Jiang et al.*, 2014].

### 2.2. Pond Identification, Tracking, and Analysis

In the binary images we identify all isolated ponds, also referred to as mudflats, bays, coastal lagoons, or marsh basins, using the Moore-Neighbor tracing algorithm [*Gonzalez et al.*, 2004]. We use the term pond in this paper to refer to all isolated, semienclosed, interior water bodies on the marsh surface, and our definition of a pond is more inclusive than solely a small (1–50 m) isolated depression on the marsh platform. Our ponds appear isolated at Landsat resolution (30 × 30 m), but subpixel water bodies (like a channel) may actually connect our ponds. We track ponds through time by minimizing the distance between centroids in successive composite images. We only track ponds that (1) are present in every composite image, (2) are larger than 7200 $m^2$, (3) have a simple geometry (see supporting information, Shape Factors [*Kalff*, 2002; *Passalacqua et al.*, 2013]), and (4) have area change over 34 years greater than 3600 $m^2$ (4 pixels). Given Landsat resolution (30 × 30 m), we exclude all ponds smaller than 7200 $m^2$ (8 pixels) and any ponds whose area change over 34 years is less than 3600 $m^2$ as 4-pixel change in area is assumed to be within detection error and excluded from our subset of expanding ponds.

We measure how ponds change area, perimeter, and centroid position through time (Figure 1b) and whether ponds merge (Figure S1 in the supporting information). The vector of centroid movement is defined by the change in centroid position between 1983 and 2016 (Figure S1). For merging ponds, we treat each pond as an individual data point. Area change for merging ponds is the difference between the final area of the merged pond in 2016 and the sum of the area in 1983 of all merged ponds (Figure S2). Enlargement of the subpixel waterbodies (like channels) may cause pond merging [e.g., *Schepers et al.*, 2017].

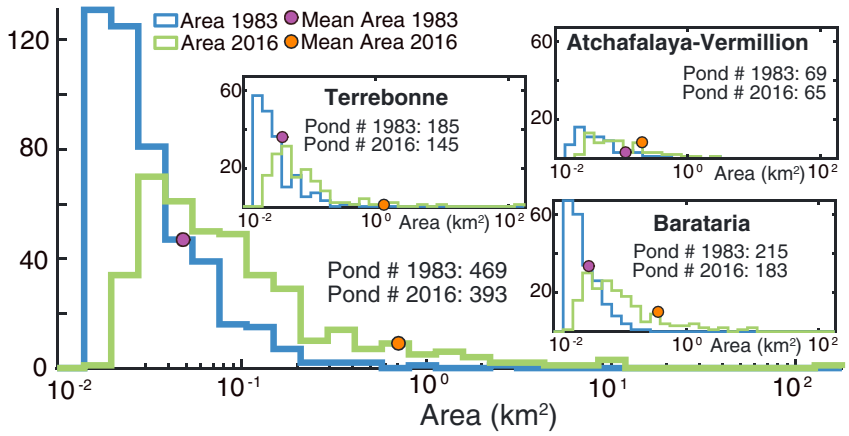


**Figure 2.** Change in number and area of ponds from 1982 to 2016. Histogram of total pond area for all basins and for each basin for 1983 (blue) and 2016 (green) with mean area denoted by filled circles (purple for 1983 and orange for 2016).

From changes in perimeter, we calculate the simple fetch, edge-retreat on each pond, and wave power. We define simple fetch as the 90th percentile of the magnitude of fetch in the direction of a given wind for all edge points on the pond [*Manual*, 1984; *Rohweder et al.*, 2012, *Karimpour et al.*, 2015] (Figure S1). We choose the 90th percentile simple fetch values as a representative maximum distance that drives wave generation. Edge-retreat rate for each pond is calculated by dividing the total area change from 1983 to 2016 by the perimeter in 2016 and the number of years (Figure S1). Based on our simple fetch values and weighted relevant wind, we calculate fetch-limited wave power for each pond using *Young and Verhagen* [1996] method (see supporting information, Wave Equations [*Eckart*, 1952; *Swart*, 1974]).

## 3. Results

### 3.1. Identifying, Tracking, and Quantifying Pond Behavior

We tracked 730 ponds from the three basins and visually confirmed the centroid of each pond in Google Earth. We found that 64% of ponds are expanding ($n$ = 469), 19% are contracting ($n$ = 142), and 16% change less than 3600 $m^2$ ($n$ = 119). At a basin scale, in Atchafalaya-Vermillion ($n$ = 208) 34% of ponds are expanding and 31% are contracting. In Terrebonne ($n$ = 250), 81% are expanding and 7% are contracting. In Barataria ($n$ = 272), 87% are expanding and 6% are contracting. For the 469 expanding ponds in the three basins, total pond area and average pond size increase—even though pond number decreases—because ponds are expanding and merging (Figure 2). In fact, 25% of the 469 expanding ponds merge into larger ponds (115 ponds merge into 39 ponds). However, only 10% of the ponds ($n$ = 7) in Atchafalaya-Vermillion merge, while in Terrebonne and Barataria basins 30% and 25% ($n$ = 55 and 53) of ponds merge.

The change in pond area, calculated as expansion minus contraction, over the 34 year period accounts for 17% (250 $km^2$) of net land loss across the whole MRDP from 1983 to 2015 (1425 $km^2$) [*Couvillion et al.*, 2011]. The 354 nonmerging expanding ponds account for 2.2% (34 $km^2$) of net land loss, while the 115 merging expanding ponds account of for 15% (218 $km^2$).

Ponds are expanding in a preferential direction of 201° (Figure 3). Expansion direction, defined by centroid movement, is distributed nonuniformly around the circle, and the resultant direction is statistically significant (V-test, $p = 9.5 \times 10^{-4}$, $n$ = 469) [*Zar*, 1999; *Berens*, 2009] (Figure 3). Similarly, ponds in individual basins are expanding 270°, 198°, and 252° in Atchafalaya-Vermillion, Terrebonne, and Barataria, respectively ($n$ = 69, 185, and 215, respectively). We treat merging ponds individually when we calculate centroid movement.

Remarkably, we find that ponds are expanding in a direction similar to the dominant winds (Figure 3). The resultant mean wind magnitude and direction, weighted by wind velocity square, is 7.0 m/s blowing toward 251° (see supporting information for more information on Wind Data [*Jensen and U. S. A. C. of Engineers*, 2010]).

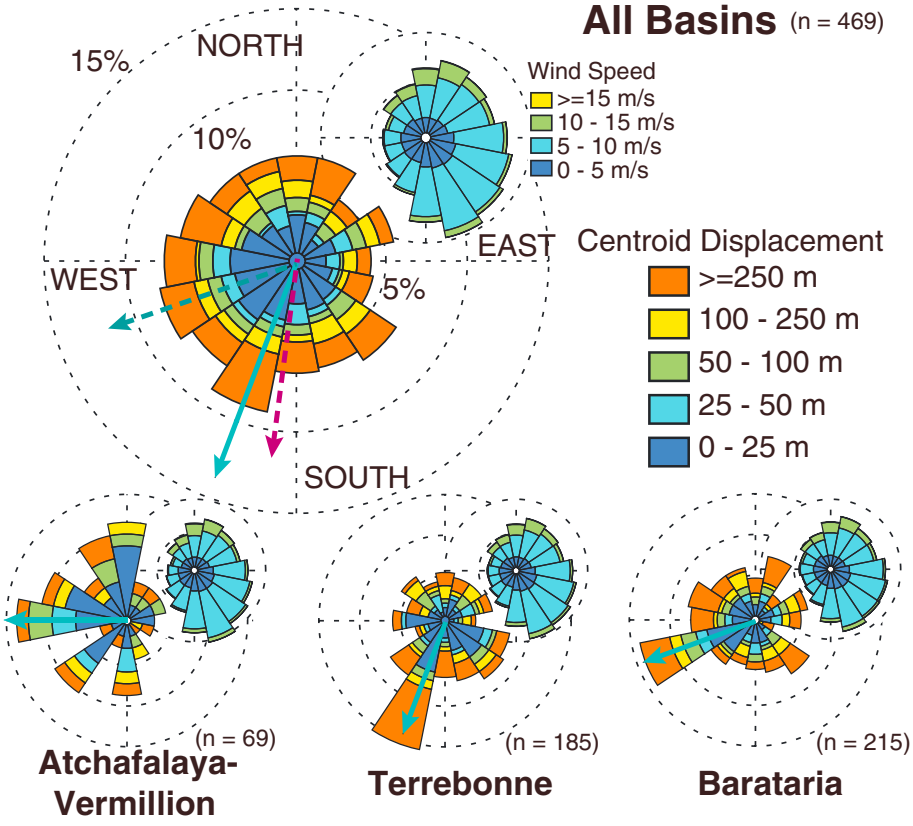


**Figure 3.** Pond centroids are moving in a similar direction as the dominant winds. Rose diagrams of centroid movement. Centroid movement is defined as the angle between the 1983 and 2016 centroid position. The 30 year wind rose for each basin is inset. The solid arrows indicate mean direction of centroid movement for all ponds (teal). The dashed arrows indicate weighted mean wind direction for all winds (teal) and winds greater than 10 m/s (magenta). Note that wind rose diagrams are displayed in standard meteorological convention depicting the directions that the winds are coming from.

The weighted resultant mean magnitude and direction of strong winds (>10 m/s) is 11.9 m/s blowing toward 191° (Figure 3). These directions bracket the pond expansion direction of 201° (Figure 3). Moreover, there are few ponds expanding toward the NE quadrant, which contains low wind energy. In Terrebonne, the ponds are expanding in a direction similar to the maximum winds, while in Barataria, ponds are expanding in a direction similar to the mean wind.

We find that larger ponds have faster rates of centroid movement, which creates the larger area change (Figure 4a). The largest area ponds are dominated by merging ponds (indicated by ponds with the same 2016 area and same total area change as denoted by the same color) for all three basins. This occurs because as pond size increases, ponds frequently merge with other waterbodies on the marsh [*Mariotti*, 2016]. Pond merging defines the data range but not the pattern. If we remove all pond merges, the functional relationship is the same.

### 3.2. Connecting Pond Behavior to Wind-Driven Waves

The striking correspondence between pond expansion directions and dominant wind directions suggests that the two are related. To connect pond behavior to wind-driven wave edge-erosion, we calculate the simple fetch in the direction of weighted maximum mean wind (191°). If ponds are deforming by wind-driven waves, the length of simple fetch should increase with time. Indeed, we see that for increasing centroid movement, the simple fetch also increases (Figure 4b). Using simple fetch measured in 2016 and weighted mean maximum wind speed (11.9 m/s), we calculate potential wave power [*Young and Verhagen*, 1996], assuming a characteristic pond depth of 0.5 m [*Mariotti*, 2016]. We find that ponds with longer simple fetch may have larger centroid movement because the waves can erode the marsh edges (Figure 4c)

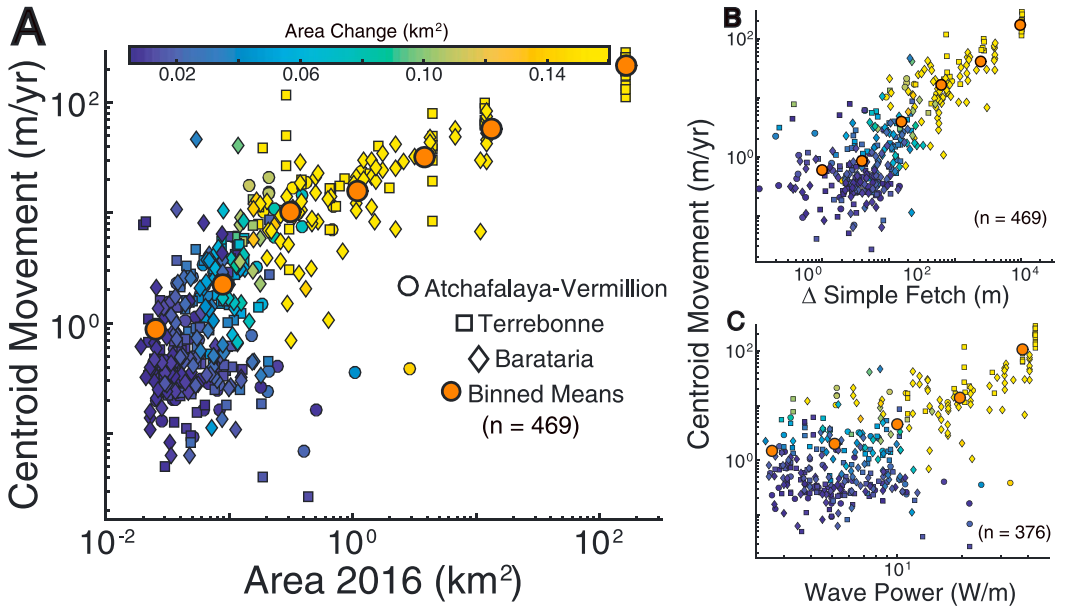


**Figure 4.** Connecting pond behavior to wind-driven wave dynamics. (a) Centroid movement versus 2016 area for all expanding ponds for each basin. (b and c) Centroid movement is positively correlated to changes in simple fetch and wave power. Change in simple fetch is the difference along the direction of weighted mean maximum winds from 1983 to 2016 for all expanding ponds. Wave power is calculated from 2016 simple fetch and weighted mean maximum wind (11.9 m/s). In every plot, evenly distributed, log-spaced mean values (orange circles) illustrate trends in data, and data points are colored by magnitude of area change.

based on critical shear stress (0.1 Pa) for erosion [*Mariotti and Fagherazzi*, 2010, 2013; *Leonardi et al.*, 2015; *Mariotti*, 2016].

### 3.3. Pond Behavior and Runaway Expansion

Recent theory predicts that ponds larger than a critical width of 200 to 1000 m are susceptible to runaway expansion due to the positive feedback between increasing fetch and wave size [*Mariotti and Fagherazzi*,

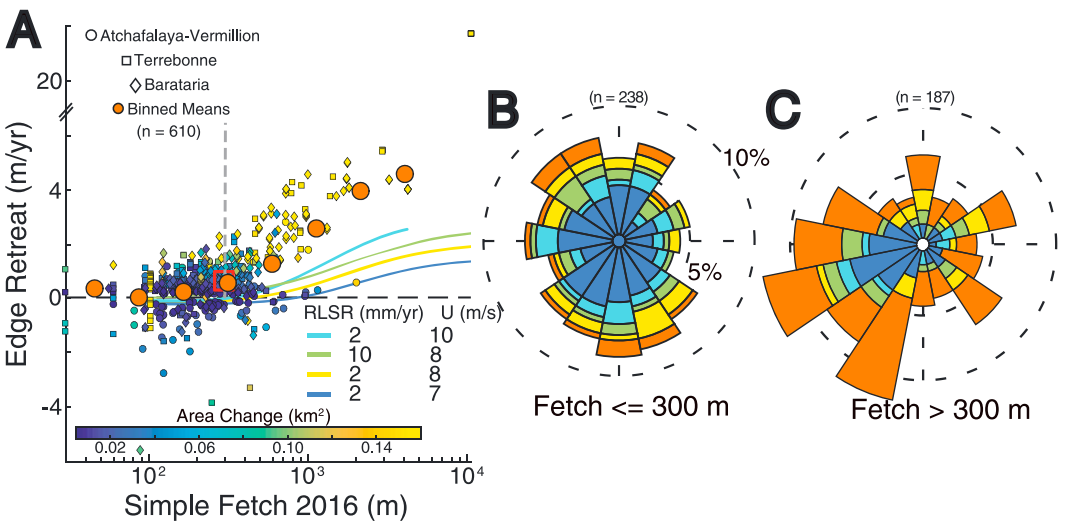


**Figure 5.** Edge retreat increases rapidly for ponds wider than 300 m. (a) Edge retreat rate for all expanding and contracting ponds versus simple fetch for 2016. Notice break in *y* axis scale. The solid lines are theoretical predictions [*Mariotti and Fagherazzi*, 2013] for a range of wind speeds (U) and sea level rise rates (RSLRs) with sediment concentration of 30 mg/L and tidal range of 1.4 m. Evenly distributed, log-spaced mean values (orange circles) illustrate trends in data. (b and c) Rose diagrams of pond expansion for all expanding ponds with simple fetch less than 300 m and greater than 300 m using same color scheme as Figure 3.

2013; *Mariotti*, 2016]. To find the critical pond width in our field data, we examine the change in edge-retreat rate as a function of simple fetch, which is the relevant pond width. We calculate edge-retreat rate (Figure S1) for all expanding and contracting ponds that change by more than 3600 $m^2$ (Figure 5a). We find that edge-retreat rate is near zero for ponds less 300 m wide and rapidly increases above 300 m and reaches an edge-retreat rate of 5 m/yr (Figures 5b and 5c).

Because marsh edge erosion increases rapidly above a simple fetch of 300 m, we designate it the critical width (Figure 5a). Consistent with this interpretation, we see that the expanding ponds wider than 300 m are more clearly moving in the dominant wind-direction (Figure 5c) compared to the distribution of all expanding ponds (all basins; Figure 3). Ponds smaller than 300 m have a uniform distribution around the circle and no statistically significant expansion direction, based on circular statistics at the 95% confidence level (V-test, $p = 0.077$, $n = 238$). Admittedly, the $P$ value is close to critical. The lack of a clear expansion direction for small ponds suggests that they are not controlled by wind-driven wave edge-erosion and instead are dominated by other processes, such as soil creep, which may lack a preferential direction [*Day et al.*, 2011; *Mariotti et al.*, 2016]. *Mariotti* [2016] found that isolated small ponds (<100 m) may be drained when hydrologically connected by a tidal channel similar to *Wilson et al.* [2014] finding a "pond cycle" of formation, expansion, drainage, and recovery of smaller ponds.

## 4. Discussion

We interpret our data to show that ponds are expanding due to wind-driven wave edge-erosion (Figure 4). After all, ponds are predominantly moving in the direction of the dominant winds (Figure 3), and ponds with larger areas and longer simple fetch distances moved faster (Figures 4a and 4b) because they are generating larger waves that erode the edges more quickly (Figures 4c and 5a). That said, we cannot rule out the importance of drowning. Pond expansion from drowning is likely due to subsidence [*Morton et al.*, 2003]. Using regional subsidence measured from 1922 to 1995 across the MRDP, we calculate an average subsidence of 11–13 mm/yr for our three basins (data from Figure 5 [*Zou et al.*, 2015]). The average basin rate of subsidence does not explain the differences in average basin edge-erosion rates (Figures 3 and 4). Nonetheless, subsidence may be enhancing our measured edge-retreat rates, which are higher than theoretical predictions under similar sediment input and wind conditions (compare data points and solid lines in Figure 5a).

Based on pond behavior, we suggest that the Atchafalaya-Vermillion basin is quasi-stable, whereas the ponds in Terrebonne and Barataria basins are undergoing runaway expansion (Figure 5a). Terrebonne and Barataria have a net land loss from pond expansion of 185 $km^2$ and 61 $km^2$, respectively, compared to only 4 $km^2$ in Atchafalaya-Vermillion. Over the study period, ponds in Atchafalaya-Vermillion have an average edge-erosion rate of 1.0 m/yr and average simple fetch of 328 m ($n = 69$), near the critical width (Figure 5a), suggesting that ponds are quasi-stable. In Terrebonne and Barataria, the average edge-erosion rates are 9.3 m/yr and 2.7 m/yr, while the average simple fetch distances are 1340 m ($n = 185$) and 590 m ($n = 215$), respectively. These average fetch distances are well above the critical width, suggesting runaway expansion for these ponds. These results agree with theory [*Mariotti*, 2016] that also predicts runaway pond expansion for sites in Barataria and Terrebonne basins while predicting pond recovery for sites in Atchafalaya-Vermillion. *Schepers et al.* [2017] found that the area on the marsh containing larger ponds (larger fetch) has the highest proportion of land covered by open water. This result agrees with the behavior of the larger fetch ponds dominating total land loss.

The difference in pond behavior between these basins is certainly due in part to higher sediment supply in Atchafalaya-Vermillion compared to Terrebonne or Barataria [*Reed*, 2002; *Blum and Roberts*, 2012; *Mariotti*, 2016; *Twilley et al.*, 2016]. However, another important attribute may be pond density on the marsh surface. Pond density (defined as the number of ponds relative to total land area) in Barataria and Terrebonne was 4 times higher in 1983 than Atchafalaya-Vermillion. Regardless of sediment supply differences, favorable conditions existed for frequent pond merging, leading to larger ponds and higher edge retreat rates (Figure 5a). Previous work has correlated higher connectivity of ponds to increased land loss [*Schepers et al.*, 2017]; even though Landsat resolution is too coarse to accurately measure pond connectivity, higher pond density for Terrebonne and Barataria than Atchafalaya-Vermillion may indicate increased pond connectivity in 1983 for both basins compared to Atchafalaya-Vermillion.

## 5. Conclusions

We tracked 730 ponds on the Mississippi River Deltaic Plain (MRDP) from 1982 to 2016 to understand how they are changing shape and size. Our results show that 64% of ponds ($n$ = 469) are expanding. The expansion direction is predominantly toward the SW (201°), which is similar to the dominant wind direction. To connect pond expansion direction to wind-driven wave edge-erosion, we calculate the wave power generated by the dominant winds on each pond. Ponds with larger fetch distances experience more expansion because they have higher wave power that erodes the marsh edge. Not all ponds in the MRDP are rapidly expanding, however. Measuring all 730 ponds, we find that 300 m is a critical width because edge-retreat rate is near zero for ponds less 300 m wide and rapidly increases above 300 m. Moreover, ponds with a fetch larger than 300 m ($n$ = 218) account for 94% of total net land loss on the marsh (236 $km^2$ of 250 $km^2$). Furthermore, expanding ponds in Atchafalaya-Vermillion basin within the MRDP have slow edge retreat rates of 1.0 m/yr and the average pond width measured along the wind direction is 328 m. Whereas in Barataria and Terrebonne basins the average edge-retreat rates are 9.3 m/yr and 2.7 m/yr, respectively, and the average simple fetch distances are 1340 m and 590 m. These results suggest that Atchafalaya-Vermillion may be quasi-stable to edge erosion in ponds, whereas Barataria and Terrebonne may experience accelerating rate of edge erosion.

**Acknowledgments**

We would like to thank J. Arcuri for her help in checking pond centroids in Google Earth. We would like to thank G. Mariotti and M. Kirwan for their helpful reviews. Funding: We acknowledge support from NSF (grants 1426997 and 1135427) and from the National Center for Earth Surface Dynamics 2 Postdoctoral Synthesis Fellowship. Author contributions: A.C.O. and D.A.E. conceived of and designed the experiments, S.R. contributed to composite creation, and all authors analyzed the data and wrote the paper. Competing interests: The authors declare that they have no competing interests. Data and material availability: Data used in making all figures are available in Table S1, and codes referenced in the paper are available upon request from A.C.O.

## References

Allison, M., Q. J. Chen, B. Couvillion, A. Freeman, M. Leadon, A. McCorquodale, E. Meselhe, C. Ramatchandirane, D. Reed, and E. White (2017), *2017 Coastal Master Plan Attachment C3–2 : Marsh Edge Erosion*, pp. 1–40, Rouge, Baton.

Berens, P. (2009), CircStat: A MATLAB toolbox for circular statistics, *J. Stat. Software*, *31*(10), 1–21.

Blum, M. D., and H. H. Roberts (2012), The Mississippi Delta region: Past, present, and future, *Annu. Rev. Earth Planet. Sci.*, *40*(1), 655–683, doi:10.1146/annurev-earth-042711-105248.

Chander, G., B. L. Markham, and D. L. Helder (2009), Summary of current radiometric calibration coefficients for Landsat MSS, TM, ETM+, and EO-1 ALI sensors, *Remote Sens. Environ.*, *113*(5), 893–903.

Couvillion, B. R., and H. Beck (2013), Marsh collapse thresholds for coastal Louisiana estimated using elevation and vegetation index data, *J. Coastal Res. Spec. Issue*, *63*(63), 58–67, doi:10.2112/SI63-006.1.

Couvillion, B. R., J. A. Barras, G. D. Steyer, W. Sleavin, M. Fischer, H. Beck, N. Trahan, B. Griffin, and D. Heckman (2011), Land area change in coastal Louisiana (1932 to 2010) 529.

Craft, C., J. Clough, J. Ehman, S. Joye, R. Park, S. Pennings, H. Guo, and M. Machmuller (2009), Forecasting the effects of accelerated sea-level rise on tidal marsh ecosystem services, *Front. Ecol. Environ.*, *7*(2), 73–78.

Day, J. W., G. P. Kemp, D. J. Reed, D. R. Cahoon, R. M. Boumans, J. M. Suhayda, and R. Gambrell (2011), Vegetation death and rapid loss of surface elevation in two contrasting Mississippi delta salt marshes: The role of sedimentation, autocompaction and sea-level rise, *Ecol. Eng.*, *37*(2), 229–240.

DeLaune, R. D., J. A. Nyman, and W. H. Patrick Jr. (1994), Peat collapse, ponding and wetland loss in a rapidly submerging coastal marsh, *J. Coastal Res.*, 1021–1030.

Donchyts, G., J. Schellekens, H. Winsemius, E. Eisemann, and N. van de Giesen (2016a), A 30 m resolution surface water mask including estimation of positional and thematic differences using Landsat 8, SRTM and OpenStreetMap: A case study in the Murray-Darling Basin, Australia, *Remote Sens.*, *8*(5), 386.

Donchyts, G., F. Baart, H. Winsemius, N. Gorelick, J. Kwadijk, and N. van de Giesen (2016b), Earth's surface water change over the past 30 years, *Nat. Clim. Change*, *6*(9), 810–813.

Dong, J., X. Xiao, M. A. Menarguez, G. Zhang, Y. Qin, D. Thau, C. Biradar, and B. Moore III (2016), Mapping paddy rice planting area in northeastern Asia with Landsat 8 images, phenology-based algorithm and Google Earth Engine, *Remote Sens. Environ.*, doi:10.1016/j.rse.2016.02.016.

Eckart, C. (1952), The propagation of gravity waves from deep to shallow water, in *Proceedings of the NBS Semicentennial Symposium on Gravity Waves*, vol. Circular 5, edited by N. B. of Standards, p. 165, NBS.

Edmonds, D. A. (2012), Restoration sedimentology, *Nat. Geosci.*, *5*(11), 758–759.

Fagherazzi, S., G. Mariotti, P. Wiberg, and K. McGlathery (2013), Marsh collapse does not require sea level rise, *Oceanography*, *26*, 70–77.

Flood, N. (2013), Seasonal composite landsat TM/ETM+ images using the medoid (a multi-dimensional median), *Remote Sens.*, *5*(12), 6481–6500, doi:10.3390/rs5126481.

Gautam, V. K., P. K. Gaurav, P. Murugan, and M. Annadurai (2015), Assessment of surface water dynamics in Bangalore using WRI, NDWI, MNDWI, supervised classification and K-T transformation, *Aquat. Procedia*, *4*, 739–746, doi:10.1016/j.aqpro.2015.02.095.

Gonzalez, R., R. Woods, and S. Eddins (2004), *Digital Image Processing Using Matlab*, chap. 10, pp. 378–425, Pearson Prentice Hall, Upper Saddle River, N. J.

Griffiths, P., T. Kuemmerle, M. Baumann, V. C. Radeloff, I. V. Abrudan, J. Lieskovsky, C. Munteanu, K. Ostapowicz, and P. Hostert (2014), Forest disturbances, forest recovery, and changes in forest types across the Carpathian ecoregion from 1985 to 2010 based on Landsat image composites, *Remote Sens. Environ.*, *151*, 72–88.

Jensen, R. E. (2010), *Wave Information Studies*, edited by U. S. A. C. of Engineers. [Available at http://wis.usace.army.mil/.]

Jiang, H., M. Feng, Y. Zhu, N. Lu, J. Huang, and T. Xiao (2014), An automated method for extracting rivers and lakes from Landsat imagery, *Remote Sens.*, *6*(6), 5067–5089, doi:10.3390/rs6065067.

Kalff, J. (2002), *Limnology: Inland Water Ecosystems*, Prentice Hall, Upper Saddle River, N. J.

Karimpour, A., Q. Chen, and R. R. Twilley (2015), A Field Study of How Wind Waves and Currents May Contribute to the Deterioration of Salmarsh Fringe, *Estuaries Coasts*, doi:10.1007/s12237-015-0047-z.

Kirwan, M. L., and J. P. Megonigal (2013), Tidal wetland stability in the face of human impacts and sea-level rise, *Nature*, *504*(7478), 53–60.

Kirwan, M. L., S. Temmerman, E. E. Skeehan, G. R. Guntenspergen, and S. Fagherazzi (2016), Overestimation of marsh vulnerability to sea level rise, *Nat. Clim. Change*, *6*(3), 253–260.

Kuleli, T., A. Guneroglu, F. Karsli, and M. Dihkan (2011), Automatic detection of shoreline change on coastal Ramsar wetlands of Turkey, *Ocean Eng.*, *38*(10), 1141–1149, doi:10.1016/j.oceaneng.2011.05.006.
Leonardi, N., N. K. Ganju, and S. Fagherazzi (2015), A linear relationship between wave power and erosion determines salt-marsh resilience to violent storms and hurricanes, *Proc. Natl. Acad. Sci. U.S.A.*, *113*(1), 64–68, doi:10.1073/pnas.1510095112.
Manual, S. P. (1984), Coastal Engineering Research Center, Dep. Army, Waterw. Exp. Stn., 1.
Mariotti, G. (2016), Revisiting salt marsh resilience to sea level rise: Are ponds responsible for permanent land loss?, *J. Geophys. Res. Earth Surf.*, *121*, 1391–1407, doi:10.1002/2016JF003900.
Mariotti, G., and S. Fagherazzi (2010), A numerical model for the coupled long-term evolution of salt marshes and tidal flats, *J. Geophys. Res.*, *115*, F01004, doi:10.1029/2009JF001326.
Mariotti, G., and S. Fagherazzi (2013), Critical width of tidal flats triggers marsh collapse in the absence of sea-level rise, *Proc. Natl. Acad. Sci. U.S.A.*, *110*(14), 5353–5356, doi:10.1073/pnas.1219600110.
Mariotti, G., W. S. Kearney, and S. Fagherazzi (2016), Soil creep in salt marshes, *Geology*, *44*(6), 459–462.
McFeeters, S. K. (1996), The use of the normalized difference water index (NDWI) in the delineation of open water features, *Int. J. Remote Sens.*, *17*(7), 1425–1432, doi:10.1080/01431169608948714.
Moore, R. T., and M. C. Hansen (2011), Google Earth Engine: A new cloud-computing platform for global-scale Earth observation data and analysis, in *AGU Fall Meeting Abstracts*, vol. 1, p. 1.
Morris, J. T., P. V. Sundareshwar, C. T. Nietch, B. Kjerfve, and D. R. Cahoon (2002), Responses of coastal wetlands to rising sea level, *Ecology*, *83*(10), 2869–2877.
Morton, R. A., G. Tiling, and N. F. Ferina (2003), Causes of hot-spot wetland loss in the Mississippi delta plain, *Environ. Geosci.*, *10*(2), 71–80.
Nyman, J. A., and R. D. DeLaune (1999), Four potential impacts of global sea-level rise on coastal marsh stability, *Curr. Top. Wetland Biogeochem.*, *3*, 112–117.
Nyman, J. A., M. Carloss, R. D. DeLaune, and W. H. Patrick (1994), Erosion rather than plant dieback as the mechanism of marsh loss in an estuarine marsh, *Earth Surf. Processes Landforms*, *19*(1), 69–84.
Otsu, N. (1975), A threshold selection method from gray-level histograms, *Automatica*, *11*(285–296), 23–27.
Passalacqua, P., S. Lanzoni, C. Paola, and A. Rinaldo (2013), Geomorphic signatures of deltaic processes and vegetation: The Ganges-Brahmaputra-Jamuna case study, *J. Geophys. Res. Earth Surf.*, *118*, 1838–1849, doi:10.1002/jgrf.20128.
Penland, S., L. Wayne, L. D. Britsch, S. J. Williams, A. D. Beall, and V. C. Butterworth (2000), Process classification of coastal land loss between 1932 and 1990 in the Mississippi River Delta Plain, southeastern Louisiana, U.S. Geol. Surv. Open File Rep., 00-0418.
Reed, D. J. (2002), Sea-level rise and coastal marsh sustainability: Geological and ecological factors in the Mississippi delta plain, *Geomorphology*, *48*(1–3), 233–243, doi:10.1016/S0169-555X(02)00183-6.
Rohweder, J., B. L. Rogala, D. Johnson, S. Anderson, F. Clark, D. Chamberlin, K. Potter, and K. Runyon (2012), Application of wind fetch and wave models for habitat rehabilitation and enhancement projects—2012 update, U.S. Army Corp. Eng. Contract Rep.
Rokni, K., A. Ahmad, A. Selamat, and S. Hazini (2014), Water feature extraction and change detection using multitemporal landsat imagery, *Remote Sens.*, *6*(5), 4173–4189, doi:10.3390/rs6054173.
Roy, D. P., J. Ju, K. Kline, P. L. Scaramuzza, V. Kovalskyy, M. Hansen, T. R. Loveland, E. Vermote, and C. Zhang (2010), Web-enabled Landsat Data (WELD): Landsat ETM+ composited mosaics of the conterminous United States, *Remote Sens. Environ.*, *114*(1), 35–49, doi:10.1016/j.rse.2009.08.011.
Schepers, L., M. Kirwan, G. Guntenspergen, and S. Temmerman (2017), Spatio-temporal development of vegetation die-off in a submerging coastal marsh, *Limnol. Oceanogr.*, *62*(1), 137–150, doi:10.1002/lno.10381.
Steyer, G. D., B. R. Couvillion, and J. A. Barras (2013), Monitoring vegetation response to episodic disturbance events by using multitemporal vegetation indices, *J. Coastal Res.*, *63*(63), 118–130, doi:10.2112/SI63-007.1.
Swart, D. H. (1974), Offshore sediment transport and equilibrium beach profiles.
Team, G. E. E. (2015), Google Earth Engine: A planetary-scale geo-spatial analysis platform.
Twilley, R. R., et al. (2016), Co-evolution of wetland landscapes, flooding, and human settlement in the Mississippi River Delta Plain, *Sustainability Sci.*, *11*(4), 711–731, doi:10.1007/s11625-016-0374-4.
Wilson, C. A., Z. J. Hughes, D. M. FitzGerald, C. S. Hopkinson, V. Valentine, and A. S. Kolker (2014), Saltmarsh pool and tidal creek morphodynamics: Dynamic equilibrium of northern latitude saltmarshes?, *Geomorphology*, *213*, 99–115, doi:10.1016/j.geomorph.2014.01.002.
Xu, H. (2006), Modification of normalised difference water index (NDWI) to enhance open water features in remotely sensed imagery, *Int. J. Remote Sens.*, *27*(14), 3025–3033, doi:10.1080/01431160600589179.
Young, I. R., and L. A. Verhagen (1996), The growth of fetch limited waves in water of finite depth. Part 1. Total energy and peak frequency, *Coastal Eng.*, *29*(1), 47–78.
Zar, J. H. (1999), *Biostatistical Analysis*, 4th ed., Chapter 27: Circular Distributions: Hypothesis Testing, Prentice Hall, Upper Saddle River, N. J.
Zou, L., J. Kent, N. Lam, H. Cai, Y. Qiang, and K. Li (2015), Evaluating land subsidence rates and their implications for land loss in the Lower Mississippi River Basin, *Water*, *8*(1), doi:10.3390/w8010010.